AIAA-2001-3749

CYCLE ANALYSIS FOR QUIETER SUPERSONIC TURBOFAN ENGINES

Marco Debiasi* and Dimitri Papamoschou †
Department of Mechanical and Aerospace Engineering
University of California, Irvine
Irvine, CA 92697-3975

Abstract

Potential development of supersonic business jets and military platforms has spurred renewed interest in solving the noise problems inherent to such aircraft. At takeoff and low altitude flight the most annoying noise components derive from jet engine exhausts that create noise levels above those permitted by current regulations. Quieter engines can be obtained by modifying current turbofan designs to create a secondary flow that suppresses noise emitted toward the ground.

In this work we outline the principal features of such an engine and compare its characteristics with those of more conventional designs. Results of a preliminary analysis of the engine cycles indicates good performance for all key segments of flight, including takeoff, transonic acceleration, and supersonic cruise. Subscale noise measurements at the exhaust conditions calculated by the cycle analysis show significant benefits in actual and perceived noise levels relative to those of the baseline engine.

I. Introduction

Jet noise remains an acute environmental problem that seeks advanced solutions, especially in the case of high-speed aircraft. Since the work of Westley and Lilley [1] on corrugated nozzles in the early 1950's, tremendous effort has been devoted to silencing jet engines. These endeavors have been very successful in subsonic aircraft with the advent of high-bypass-ratio turbofan engines. Supersonic jet noise reduction, however, remains a problem that has impeded the wide-scale development of supersonic air travel. Nevertheless, interest has been shown recently for the development of supersonic business aircraft, an indication that supersonic transport can have a niche in a market where time saving often results in crucial financial benefits. Development of a supersonic business aircraft would leverage the extensive know-how and technologies developed for military airplanes, but hinges on effective reduction of take-off noise generated by supersonic jets exhausting from the engines of such aircraft.

High-speed jet noise is dominated by Mach wave emission, which arises when turbulent eddies in the jet travel with supersonic velocity relative to the surrounding medium [2, 3]. This phenomenon has been the subject of numerous analytical, computational, and experimental investigations [4, 5, 6, 7]. In addition to Mach-wave noise, high level acoustic emission (screech and broadband noise) also occurs in jets with strong shocks, i.e., in under- or over-expanded jets [8, 9, 10, 11, 12]. This component of noise can be substantially removed by operating the jet at pressure-matched conditions. Turbulent mixing noise, manifested as Mach wave emission in high-speed jets, is by far the most difficult noise source to be controlled.

Several concepts have been developed to reduce high-speed jet noise, usually involving efforts to enhance the mixing between the jet and the surrounding air. These methods reduce the length of the high velocity region of the jet where noise is generated or confine the noise in some way [13, 14]. Unfortunately, the noise benefits produced by these techniques are accompanied by appreciable thrust and weight penal-

*Post graduate researcher, member AIAA
†Professor, Senior member AIAA

ties [15, 16]. Other solutions, like the Inverted Velocity Profile (IVP) [17, 18], supersonic plug nozzles [19], or a Thermal Acoustic Shield [20] have shown some encouraging results but have not found wide implementation.

Recently it has been shown that surrounding a supersonic jet with a secondary stream of proper characteristics inhibits the formation of Mach waves [21, 22]. Microphone surveys [23] showed that Mach waves constitute at least 85% of the far-field jet noise to which humans are most sensitive. Subsequent experiments in over- and under-expanded, coaxial high-speed jets [24] provided a better understanding of the noise dependence on the characteristics of the dual-stream configuration and proved the value of secondary flow in reducing the Mach-wave noise in imperfectly-expanded jets. Additional studies focused on directional suppression of jet noise [25] and the applicability of the suppression concept to jet engines [26].

The purpose of the present work is to show that it is possible to design an engine that reduces takeoff noise with directional suppression of Mach waves while maintaining adequate performance to propel efficiently a supersonic business jet (SSBJ) or military platform. Furthermore we show that this engine can be derived from current production military turbofans. To this aim a preliminary analysis of the engine cycle has been done to verify the viability of the dual-stream configuration at takeoff and to estimate the engine performance at various flight conditions. Experimental simulation of the jet engine exhaust has been used to predict the far-field noise and to assess the effectiveness of the method.

II. Targeted Mach Wave Elimination

Mach waves are generated by turbulent eddies that propagate in the jet with convective velocity U_c supersonic with respect to the surrounding air stream, as sketched in Fig. 1 (a). The principle of Mach Wave Elimination is to make the eddy motions of the jet subsonic with respect to their surrounding stream by shielding the jet exhaust with a suitable secondary flow. An empirical model for the secondary flow properties is based on direct measurements of the eddy convective velocity in supersonic shear layers and round jets [27]. With the configuration depicted in Fig. 1 (b), eddies of the primary flow are subsonic with respect to the secondary flow while the eddies of the latter are also subsonic with respect to the ambient air stream. In Figs. 1 and 2, subscript p denotes the primary-stream properties, s the secondary-stream properties, and ∞ the ambient air-stream properties. The symbol U represents the flow velocity, a the speed of sound, $M = U/a$ the Mach number and U_c the eddy convective velocity. Since all eddy motions are subsonic, Mach wave emission is suppressed.

Laboratory experiments with subscale coaxial nozzles, Fig. 2 (a), have shown that surrounding a supersonic jet with a secondary stream of proper characteristics inhibits radiation of Mach waves and the resulting noise [21, 23, 24]. In particular, the peak far-field noise emission is insensitive to the nozzle pressure ratio and depends primarily on the values of the Mach number and velocity in the fully-expanded region of the jet potential core. This holds for both single and dual-stream jets.

Use of eccentric nozzles, Fig. 2 (b), mitigates the elongation of the potential core that otherwise occurs when the secondary flow is annular [28]. This means that the noise source region is not appreciably lengthened with application of the secondary flow. Consequently, the secondary flow shields the noise source region much more effectively than in a concentric configuration. A related benefit is that shielding is concentrated in the direction that really matters, i.e., toward the ground. This method, called Targeted Mach Wave Elimination (TMWE), produces substantial reductions (around 12 dB) in the perceived noise emitted in the downward arc of a high-speed jet [25]. Refinements of the TMWE method using a secondary stream issued by a nozzle with arcuate shape, Fig. 2 (c), are expected to produce even larger noise reduction.

III. Aircraft and Engine Definitions

The engine cycle analysis is based on the performance of a twin-engine supersonic aircraft with takeoff weight of 100,000 lb. The aircraft is assumed to have lift-to-drag ratios $\mathcal{L}/\mathcal{D}$ of 5 at takeoff and 10 at supersonic cruise, values similar to those of the Aerospatiale Concorde. Engines for this aircraft could be designed using the core (compressor, burner, and turbine) of current low-bypass turbofans in the class 22,000-lbf dry-thrust at sea-level. Typically,

these engines have bypass ratio BPR ≈ 0.5, fan pressure ratio FPR ≈ 5, overall pressure ratio across the fan and compressor stages OPR $\approx 25-30$, turbine entry temperature TET = 1,700-1,800 K, and core mass flow rate 90-110 lb/s. Such an engine is the Pratt & Whitney F119, schematized in Fig. 3 (a), whose approximate model constitutes the baseline engine of this study.

Turbofan engines are very efficient at high-subsonic and moderate-supersonic speeds, but due to their secondary stream, exhibit a larger frontal cross section compared to turbojets. Turbofans are also quieter than turbojets at take-off since they obtain the same thrust by accelerating a larger amount of air at lower speed. However, at higher speed (Mach 2 or higher), turbojets are preferable because all the flow ingested is squeezed into the core, energized, and exhausted at very high velocity giving better overall engine efficiency at these flight conditions. The ideal engine for a supersonic commercial aircraft would be one that operates as a turbofan at take-off, subsonic speed and low supersonic speed, and as a turbojet at the higher cruise speed. This would entail a variable engine configuration, a concept that has already been implemented (see, for instance, the General Electric F120 variable-cycle turbofan developed for the Advanced Tactical Fighter) [29].

A conceptual layout of a supersonic business jet using TMWE engines at takeoff is shown in Fig. 4. At take-off the derivative engine, Fig. 3 (b), uses the fan stream to produce the silencing secondary stream. Given a twin spool turbofan core like that of the baseline engine, 40 % more power would be extracted from the core stream by the low pressure turbine (LPT) to drive the fan. The first, larger fan elements impel a moderate pressure ratio to an increased bypass stream. Two-fifths of this stream flows separately around the engine and exhausts in the secondary nozzle as sketched in Fig. 3 (b). The remainder proceeds through successive fan elements, splits in bypass and core flows as in the original engine, and then mixes before exhausting in the primary nozzle. During other segments of the mission, a guided vane directs the entire flow compressed by the first fan elements into the inner part of the engine, Fig. 3 (c). This is equivalent to the baseline engine with increased mass flow rate. The advantage of this design is the more efficient use of all the air-flow ingested at high-speed cruise.

Alternatively, one can mix the secondary and primary flows before expanding them through the primary nozzle, Fig. 3 (d). This configuration entails addition of a mixer at the turbine exit and is somewhat simpler that the TMWE configuration as it requires no variation of the engine geometry with the exception of the exhaust nozzle. The exhausting stream approximates the Fully Mixed Equivalent (FMEQ) of the dual-stream jet, which has been argued to be the standard against which non-mixed jets should be judged in the context of noise [30]. FMEQ represents an idealized condition that ignores non-uniformities at the exhaust profile and noise from the internal mixer.

IV. Engine Cycle Analysis

Thermodynamic analysis of the various engine variants follows the general approach presented in Hill & Peterson [31]. Subscript 0 refers to stagnation values with additional subscripts used to indicate the engine components or the state of the fluid.

Modern turbofan engines adopt a modular design that allows development of a family of different engines using the same engine core (gas generator). To compare results relative to different cycles adopting the same engine core, it is proper to non-dimensionalize the mass flow rates in each engine component with respect to the mass flow rate in the compressor. We define the ratio between the generic mass flow rate $\dot{m}$ and the mass flow rate $\dot{m}_{\rm com}$ in the compressor as

$$m_r \equiv \frac{\dot{m}}{\dot{m}_{\rm com}} \tag{1}$$

For instance, the bypass ratio BPR is equal to the fan and compressor mass flow ratio, i.e.

$$\mathrm{BPR} = m_{r_{\rm fan}} = \frac{\dot{m}_{\rm fan}}{\dot{m}_{\rm com}} \tag{2}$$

Except for the flow in the air intake and in the exhaust nozzles, the gas velocity in all the other components is small and therefore stagnation conditions are used to describe the flow. Variations of the composition of the gas (air) through the engine are considered negligible as well as the variations of specific heat c_p and c_v and of their ratio γ during *each* process. Changes of the gas specific heat with the temperature are taken into account adopting the typical values of γ suggested in [31] for each component, as summarized in Table 1.

Basic processes

Four basic processes constitute the cycle of a jet engine: compression, expansion, heat addition (combustion), and mixing.

Compression

Compression takes place in the air intake, fan, and compressor. It is a process whose adiabatic efficiency η_c is defined as

$$\eta_c = \frac{T_{0_{fs}} - T_{0_i}}{T_{0_f} - T_{0_i}} \tag{3}$$

where the subscripts i and f refer to the initial and final state of the actual process, and fs to the final state of the corresponding isentropic process.

Expansion

Expansion takes place in the engine turbine and in the exhaust nozzles. The expansion efficiency η_e is defined as

$$\eta_e = \frac{T_{0_f} - T_{0_i}}{T_{0_{fs}} - T_{0_i}} \tag{4}$$

Combustion

The efficiency η_h of the heating process occurring in the combustion chamber is defined as

$$\eta_h = \frac{\left(m_{r_f} T_{0_f} - m_{r_i} T_{0_i}\right) c_p}{m_{r_{\text{fuel}}} Q} \tag{5}$$

where Q is the heating value of jet-A fuel ($Q = 43,400$ kJ/kg). Table 1 lists the component efficiencies used in calculations.

Mixing

Mixing processes occur in the turbine between the combusted gas and cooling air bled from the compressor as well as between the core and fan streams of some engines. This is constant-pressure mixing where the momentum flux (and therefore thrust), mass flow rate, and stagnation enthalpy are preserved. Using subscripts i and j to specify two unmixed streams and subscript f for the final mixed stream, conservation of the mass flow rate gives

$$m_{r_f} = m_{r_i} + m_{r_j} \tag{6}$$

The specific heat of the mixed stream is obtained by mass-averaging those of the unmixed streams. Conservation of stagnation enthalpy gives

$$T_{0_f} = \frac{m_{r_i} c_{p_i} T_{0_i} + m_{r_j} c_{p_j} T_{0_j}}{m_{r_f} c_{p_f}} \tag{7}$$

Using

$$\dot{m} = m_r \dot{m}_{\text{com}} = pMA\sqrt{\gamma/(RT)} \tag{8}$$

where A, M, and T are the cross-sectional area, Mach number, and temperature of each stream after isentropic expansion to the reference pressure p, Eq. 6 becomes

$$\sqrt{\frac{\gamma_f}{T_f}} M_f A_f = \sqrt{\frac{\gamma_i}{T_i}} M_i A_i + \sqrt{\frac{\gamma_j}{T_j}} M_j A_j \tag{9}$$

thus

$$A_f = \frac{1}{M_f}\sqrt{\frac{T_f}{\gamma_f}}\left(\sqrt{\frac{\gamma_i}{T_i}} M_i A_i + \sqrt{\frac{\gamma_j}{T_j}} M_j A_j\right) \tag{10}$$

The momentum flux of each stream is $\dot{m}U = \gamma p M^2 A$. Conservation of momentum flux gives

$$\gamma_f M_f^2 A_f = \gamma_i M_i^2 A_i + \gamma_j M_j^2 A_j \tag{11}$$

Combining with Eq. 10, we have

$$M_f = \frac{\gamma_i M_i^2 A_i + \gamma_j M_j^2 A_j}{\sqrt{\gamma_f T_f}\left[\sqrt{\frac{\gamma_i}{T_i}} M_i A_i + \sqrt{\frac{\gamma_j}{T_j}} M_j A_j\right]} \tag{12}$$

On factoring out T_{0_f},

$$\frac{M_f}{\sqrt{1 + \frac{\gamma_f - 1}{2} {M_f}^2}} = \frac{\gamma_j M_j + \gamma_i \frac{M_i^2}{M_j}\frac{A_i}{A_j}}{\sqrt{\gamma_f T_{0_f}}\left[\sqrt{\frac{\gamma_j}{T_j}} + \sqrt{\frac{\gamma_i}{T_i}}\frac{M_i}{M_j}\frac{A_i}{A_j}\right]} \tag{13}$$

The area ratio $\frac{A_i}{A_j}$ is obtained from Eq. 8:

$$\frac{A_i}{A_j} = \frac{m_{r_i}}{m_{r_j}}\frac{M_j}{M_i}\sqrt{\frac{\gamma_j T_i}{\gamma_i T_j}} \tag{14}$$

Inserting in Eq. 13,

$$\frac{M_f}{\sqrt{1 + \frac{\gamma_f - 1}{2} {M_f}^2}} = \frac{\gamma_j M_j + \gamma_i M_i \frac{m_{r_i}}{m_{r_j}}\sqrt{\frac{\gamma_j T_i}{\gamma_i T_j}}}{\sqrt{\gamma_j \gamma_f \frac{T_{0_f}}{T_j}}\left[1 + \frac{m_{r_i}}{m_{r_j}}\right]} \equiv \beta \tag{15}$$

from which

$$M_f = \frac{\beta}{\sqrt{1 - \frac{\gamma_f - 1}{2}\beta^2}} \tag{16}$$

Once M_f is calculated, the stagnation pressure of the mixed stream is determined from the definition

$$p_0 = p\left(1 + \frac{\gamma - 1}{2} M^2\right)^{\frac{\gamma}{\gamma - 1}} \tag{17}$$

with $M = M_f$ and $\gamma = \gamma_f$.

The variation of the entropy corresponding to each of the elemental processes above is computed approximately from the thermodynamics relation

$$s_f - s_i \ = c_p \left(\frac{T_{0_f}}{T_{0_i}} \right) - R \ln \left(\frac{p_{0_f}}{p_{0_i}} \right) \qquad (18)$$

while the gas density is obtained from the equation of state

$$p \ = \rho R T \qquad (19)$$

Engine cycle

Air intake

For given ambient pressure, temperature, and Mach number, the stagnation pressure and temperature of the flow ingested by the air intake are computed by using Eq. 17 and the definition

$$T_0 \ = T \left(1 + \frac{\gamma - 1}{2} M^2 \right) \qquad (20)$$

The corresponding stagnation pressure at the fan inlet is obtained combining Eq. 3 with the isentropic relation

$$\frac{T_{0_{fs}}}{T_{0_i}} = \left(\frac{p_{0_{fs}}}{p_{0_i}} \right)^{\frac{\gamma-1}{\gamma}} \qquad (21)$$

Fan and compressor

The stagnation pressure at the exit of the fan, point 3, is defined by the stagnation pressure at the fan inlet times the fan pressure ratio. The corresponding temperature can be found by combining Eqs. 3 and 21. In similar way one can compute the flow conditions at the exit of the compressor, point 4.

Combustion chamber

Combustion losses are usually expressed in terms of the pressure drop across the combustion chamber. The pressure drop used in our analysis is 5 % [31]. The temperature at the exit of the combustor is the maximum temperature of the cycle and corresponds to the Turbine Entry Temperature. The fractional fuel mass flow required to achieve a specified TET value can be obtained from Eq. 5.

Turbine

Typically, part of the air exiting the compressor is bled and delivered to the turbine stages to form an air film that surrounds the blades and shields them from the hot combustion gas. The majority of cooling air is used in the first (hotter) turbine stages. Therefore in the turbine both mixing and expansion processes take place simultaneously. In our analysis this has been simulated by dividing the turbine expansion process into smaller processes alternated with the mixing of a fraction of the cooling air. More specifically, 30% of the bled air has been assumed to cool the high pressure turbine (HPT) stator, 45% the HPT rotor in 4 successive points, and 25% the LPT stator. At the entrance of the LPT rotor the temperature is low enough to require no cooling. Although the fractions of cooling air above do not necessarily match those used in real engine components, they model reasonably well the expansion-mixing process in a modern gas turbine. Furthermore, very little differences have been noticed in the results with slight variations of the above percentages or by dividing further the HPT expansion process. The conditions of the gas at the end of each elemental mixing are obtained as explained for the mixing process. The temperature at the end of each of the four expansion steps modeled for the HPT rotor is obtained by equating the corresponding power to one fourth of the power needed to drive the high pressure compressor. The corresponding pressure is then computed using Eq. 4 combined with Eq. 21. Similarly, the temperature at the exit of the LPT rotor is computed to match the power required to drive the fan.

Exhaust nozzles

Equations 4, 17, 20, and 21 are used to compute the stagnation and static flow parameters at the exit of each nozzle for a given design Mach number. At the nozzle exit, the velocity is

$$U = M \sqrt{\gamma R T} \qquad (22)$$

The equations for the exit areas of the primary and secondary nozzles are then

$$A_{\mathrm{p}} \ = \frac{\dot{m}_{\mathrm{p}}}{\rho_{\mathrm{p}} U_{\mathrm{p}}} \ = \frac{\dot{m}_{\mathrm{com}} m_{r_p}}{\rho_{\mathrm{p}} U_{\mathrm{p}}} \qquad (23)$$

$$A_{\mathrm{s}} \ = \frac{\dot{m}_{\mathrm{s}}}{\rho_{\mathrm{s}} U_{\mathrm{s}}} \ = \frac{\dot{m}_{\mathrm{com}} m_{r_s}}{\rho_{\mathrm{s}} U_{\mathrm{s}}} \qquad (24)$$

The overall thrust F of the engine is

$$F = F_{\mathrm{p}} + F_{\mathrm{s}} = \begin{array}{l} \dot{m}_{\mathrm{p}} U_{\mathrm{p}} + A_{\mathrm{p}} (p_{\mathrm{p}} - p_\infty) + \\ \dot{m}_{\mathrm{s}} U_{\mathrm{s}} + A_{\mathrm{s}} (p_{\mathrm{s}} - p_\infty) - \dot{m}_\infty U_\infty \end{array} \qquad (25)$$

where $\dot{m}_\infty$ denotes the mass flow rate ingested by the engine air intake. Equation 25 recast in terms of

mass ratio, combined with Eqs. 23 and 24, gives the value of the engine specific thrust ST

$$ST = \frac{F}{\dot{m}_{\rm com}} = m_{r_p}\left(U_{\rm p} + \frac{p_{\rm p}-p_\infty}{\rho_{\rm p}U_{\rm p}}\right) + m_{r_s}\left(U_{\rm s} + \frac{p_{\rm s}-p_\infty}{\rho_{\rm s}U_{\rm s}}\right) - m_{r,\infty}U_\infty \quad (26)$$

The overall thrust F corresponding to the design compressor mass flow rate $\dot{m}_{\rm com}$ is then obtained as

$$F = ST\ \dot{m}_{\rm com} \quad (27)$$

and the generic mass flow rate $\dot{m}$ in any component or point of the cycle can be computed with

$$\dot{m} = m_r\ \dot{m}_{\rm com} \quad (28)$$

The diameters $D_{\rm p}$ and $D_{\rm s}$ of the jet and coflow nozzles are respectively

$$D_{\rm p} = \sqrt{\frac{4A_{\rm p}}{\pi}} \quad (29)$$

$$D_{\rm s} = \sqrt{\frac{4(A_{\rm s}+A_{\rm p})}{\pi}} \quad (30)$$

Similarly, the dimension of other engine components have been derived from the corresponding local values of the mass flow rate, density, and velocity. Finally, the Specific Fuel Consumption SFC is computed as

$$\mathrm{SFC} = \frac{\dot{m}_{\rm fuel}}{F} \quad (31)$$

V. Subscale Noise Testing

Experiments measured the noise from jets with conditions calculated from the engine cycle analysis. Following is a brief overview of the facilities. More details can be found in earlier publications [21, 23, 25].

Dual-stream jet facility

High-speed dual-stream jets were obtained by supplying precisely-metered mixtures of helium and air to an eccentric nozzle arrangement like that shown in Fig. 2 (b). Helium-air mixtures simulate adequately the density, velocity, and speed of sound of a heated jet [32]. By regulating the mass fractions of helium and air, thereby regulating the gas constant of the mixture, we controlled the jet velocity at fixed Mach number. The inner nozzles used in this study had 12.7 mm exit diameter and design Mach numbers $M_p = 1.0$ and $M_p = 1.5$. The outer nozzle had a conical convergent shape and terminated at an exit diameter of 17.8 mm. The facility is equipped with pressure transducers that record the stagnation pressures of the primary and secondary streams.

Noise measurements

Noise measurements were conducted inside an anechoic chamber using a one-eighth inch condenser microphone (Brüel & Kjær 4138) with frequency response of 150 kHz. The microphone was mounted on a support that enabled noise measurements at a variety of radial distances from the nozzles and azimuthal angles θ with respect to the jet axis. The microphone output was corrected for the microphone frequency response, far-field response, and atmospheric absorption and was processed into narrowband Sound Pressure Level (SPL) spectra. The results were further corrected for equal-thrust comparison by geometrical scaling of the characteristic dimensions of the different jets. The overall sound pressure level OASPL was obtained by integrating the corrected narrowband spectrum between the lower and upper frequency limits resolved by the microphone. To assess the perceived noise from a jet engine, narrowband spectra were scaled up to full engine size, converted to discrete third-octave spectra and corrected for human perception by adding the standard A-weighting curve (dBA spectra).

All the spectra presented in this work refer to values obtained in the laboratory at fixed far-field distance and do not simulate the flyover of an airplane. Moreover, the effects of forward flight on the fluid mechanics and acoustics of the jets were not captured in this experiment due to the absence of a tertiary stream.

VI. Results

We present now the results of the thermodynamic cycle analysis and of the experimental acoustic reproduction of the baseline engine and its TMWE and FMEQ derivatives. Four important segments of the mission of a supersonic aircraft have been considered: takeoff, cutback/approach (reduced thrust setting), transonic acceleration, and supersonic cruise.

Takeoff

For the TMWE engine, we consider a turbofan engine with separate bypass stream produced by a fan with pressure ratio FPR=2.6. Other salient characteristics of this engine, assumed or derived from the cycle analysis at takeoff (i.e., at static, sea-level conditions), are summarized in Table 2. The same table presents corresponding values for the baseline engine and for the FMEQ derivative. Some caution should be paid to the fact that limited amount of technical data specific to the F119 was available to the authors. Therefore some of the values presented in Table 2 and following tables are based on data available for other similar state-of-the-art engines (e.g., SNECMA M-88, Eurojet EJ200 [33, 34]).

During takeoff the engines would run at the highest temperature (TET = 1,800 K) hypothesized for current turbine technologies [33, 35, 36]. Comparison of the T-s diagrams of the baseline engine and its derivatives at takeoff, Fig. 5, reveals that the core cycle (i.e., the power generation process) remains substantially the same for the three different configurations. However significant differences arise in the way the power is transferred to the exhausting streams. In the baseline turbofan the mixed core and bypass streams are accelerated to $M_p = 1.4$ and $U_{\rm p} = 700$ m/s. With similar core and "inner" bypass mass flow rates, the TMWE engine has lower temperature and pressure at the turbine exit due to the increased power extracted to drive the larger fan. This results in a slower primary stream with $M_p = 1.18$ and $U_{\rm p} = 580$ m/s. The power extracted from the core flow is used to produce the $M_s = 1.20$, $U_{\rm s} = 424$ m/s secondary flow. Mixing the TMWE primary and secondary stream produces an even slower primary stream ($M_p = 1.15$, $U_{\rm p} = 515$ m/s) for the FMEQ derivative. This is the approach typically exploited to reduce the velocity of an high speed jet. Although relatively slow, such a jet still radiates Mach waves.

All three engine configurations shown in Table 2 provide enough thrust for takeoff and initial climb of a 100,000 lb aircraft in the event of failure of one of the two engines. Note that this thrust is obtained without reheating the exhausting streams. Thanks to their higher bypass, the two derivatives present a better Specific Fuel Consumption (SFC) than the original design. However it should be noted that this parameter is relatively unimportant during takeoff due to the short duration of this event. More significant is the comparison of the engine diameters at the fan inlet and nozzle exit. In order to ingest the increased mass flow rate the two derivatives have a fan diameter 30 % larger than the baseline engine. Despite this increase, the fan diameter (1.30 m) is still reasonable for a supersonic engine. The nozzle diameters are also sufficiently low (e.g., $D_{\rm s} \approx 0.9$ m for the derivative engines). Unlike the nozzles, whose area can be adjusted to optimize the gas exhaust, the fan diameter is fixed and should represent the best compromise for different flight conditions. Control of the characteristics of the flow ingested by the fan must then be used by adjusting the air-intake geometry.

We now turn our attention to the takeoff noise characteristics. Figure 6 compares the narrowband far-field spectra determined experimentally for the three engines. Figure 6 (a) shows the spectra in the peak direction of noise emission (aft quadrant). A very large noise reduction across the whole spectrum is obtained with the TMWE configuration. The major contribution to this reduction is the suppression of Mach waves; reduction of the core velocity is a relatively minor contribution. The FMEQ configuration, which exploits only the effect of lower Mach number and velocity - without shielding by a secondary flow, is less effective. This result is consistent with earlier experiments by the authors [25]. In the lateral direction ($\theta = 100^o$) the noise benefit of the derivative engines is lower. Notice in particular that TMWE yields the same benefit as FMEQ since there are no Mach waves to silence in this direction.

The corresponding A-weighted spectra, which account for the human perception of noise, are presented in Fig. 7. TMWE reduces the perceived noise of about 21 dB in the aft quadrant with an advantage of 9-10 dB over FMEQ. In the lateral direction the derivative engines are less effective, but still deliver a reduction of about 8 dB.

The directivity of the peak values of the dBA spectra is shown in Fig. 8 (a). Again one can notice the superior performance of TMWE in the aft quadrant. The overall reduction in perceived noise (going around the entire measurement arc) is 17 dB for TMWE versus 11 dB for FMEQ. Figure 8(b) presents the directivity of the overall sound pressure level (OASPL). The trends are similar to those for the peak dBA levels, although the difference between TMWE and FMEQ is less. Although OASPL represents the total level of noise, it is not a reliable indicator of perceived noise [37].

Reduced Thrust

The reduced thrust condition approximates thrust settings for cutback and approach. Table 3 compares the characteristics of the engine configurations for an aircraft flying at Mach 0.32 at an altitude of 1,000 ft, using 50 % less thrust than at takeoff. At this condition, the engines run at a substantially lower TET (about 1,450 K) than at takeoff. Consequently the fan and compressor pressure ratios are lower and the demand for turbine cooling is less.

Comparison of the T-s diagrams, not shown here, shows that the the three engine configurations share a similar core cycle. The baseline jet ($M_p = 1.2$, $U_{\rm p} = 550$ m/s) exhausts at higher speed than the derivatives ($M_p = 1.12$, $U_{\rm p} = 530$ m/s for TMWE and $M_p = 1.05$, $U_{\rm p} = 450$ m/s for FMEQ). The exit diameters have the same values as at takeoff.

Figure 9 compares the narrowband far-field spectra at reduced power. In the direction of peak emission, Fig. 9 (a), TMWE shows a better performance than FMEQ despite the lower jet velocity of the latter, an indication that Mach waves are a strong source of noise even for moderately supersonic jets. The benefit is reduced compared to takeoff since the engines are intrinsically quieter at reduced thrust. In the lateral direction, where Mach waves are insignificant, FMEQ is about 2-3 dB quieter than TMWE thanks to its lower jet speed.

The corresponding dBA spectra, Fig. 10, show that TMWE reduces the perceived noise by about 12 dB in the direction of peak noise and by 4-5 dB in the lateral direction. FMEQ is about 3 dB louder than TMWE in the direction of peak noise and about 4 dB quieter in the lateral direction. The directivity plot of the peak value of the dBA spectrum, shown in Fig. 11 (a), shows that TMWE has an overall benefit of 10 dB relative to the baseline and 2 dB relative to FMEQ. TMWE retains an advantage even in terms of OASPL, as shown in the plot of Fig. 11(b). It is important to remember that FMEQ represents an idealized fully-mixed exhaust and neglects noise from velocity non-uniformities and from the internal mixer. The FMEQ noise emission from a real engine will be considerably louder than that measured here.

Transonic acceleration

Transonic acceleration is a critical segment of the mission of a supersonic aircraft. The extra thrust needed to overcome the high drag in this regime is usually obtained by reheating the exhaust stream. Because of its higher SFC, reheating should be kept at a minimum or, if possible, avoided. Typical transonic acceleration conditions are at an altitude of 40,000 ft and Mach 1.2. Table 4 summarizes the properties of the engines analyzed at these flight conditions. The highest allowable temperature (TET = 1,800 K) has been selected for this regime in order to obtain the maximum performance from the engine core without reheat. Comparing the results of the cycle analysis with those at cruise conditions (Table 5) indicates that all the engines are capable of attaining a transonic-acceleration thrust that is almost double the thrust at cruise. This compares favorably with the transonic acceleration-to-cruise thrust ratio (1.36) of the Rolls-Royce Olympus 593 Mk610, the engine propelling the Concorde [38]. At mass flow rates compatible with the fan dimensions and flow characteristics, best performance is achieved by operating the exhaust at pressure matched conditions. This requires enlarging the adjustable primary nozzle, Fig. 3 (c), filling (in the case of TMWE) the gap between primary and secondary nozzles and between the nozzle and the outer external cowl (see also Fig. 4). In these conditions the nozzle diameter $D_{\rm p}$ at its lip would be comparable to the fan tip diameter (1.0 m for baseline, 1.21-1.25 m for TMWE and FMEQ). The corresponding SFC is 0.91 lb/lbf h for baseline and TMWE and 0.84 lb/lbf h for FMEQ, a significantly better performance than the Concorde's engine (1.41 lb/lbf h) that, at the same conditions, must reheat the exhaust [38].

Cruise

Cruising at an altitude of 50,000 ft and Mach 2.0 the engines would run at a turbine temperature about 100 K lower than at takeoff and transonic acceleration in order to improve the turbine life. Figure 12 presents the cycle of the baseline and TMWE engines under these conditions. Table 5 shows the engine characteristics at cruise. Whatever the engine configuration, two engines produce a combined thrust in excess of 10,000 lbf, sufficient for propelling a 100,000 lb aircraft with cruise $\mathcal{L}/\mathcal{D} \approx 10$. Actually at optimal fan inlet mass flow, TMWE is somewhat oversized (9,000 lbf per engine). Lower thrust setting could be obtained for this engine by controlling the ingested mass flow with an air intake of variable geometry. In these conditions the primary nozzle opens up to its maximum allowable diameter, reaching a diameter $D_{\rm p}$ at its lip comparable with the outer diameter

of the engine cowl (1.3 m for baseline, 1.5-1.6 m for TMWE and FMEQ). The cruise SFC of the baseline and TMWE engine is 1.02 lb/lbf h, a 15 % improvement over the Olympus 593 (SFC = 1.19 lb/lbf h at same altitude and Mach number) deemed to be necessary for the economic viability of a SSBJ. In this respect the performance of FMEQ is somewhat poorer (SFC = 1.06 lb/lbf h).

VII. Conclusions

Preliminary analysis of the thermodynamic cycle of a high-performance turbofan engine incorporating the Targeted Mach Wave Elimination (TMWE) noise suppression technique has been performed. Subscale tests measured the noise from jets at conditions matching those calculated in the cycle analysis. The perceived noise was assessed in terms of the "A-weighted" decibel distribution around the jet.

Three engine configurations were compared: the baseline, patterned after the Pratt & Whitney F119 turbofan; the TMWE derivative; and the fully-mixed equivalent (FMEQ) of the TMWE. The engine core of the variants remained the same as for the baseline engine. In particular, there was no increase in the turbine inlet temperature.

At full-power takeoff, the TMWE derivative is about 17 dB quieter than the baseline engine and 6 dB quieter than the FMEQ variant. At reduced thrust setting, simulating cutback or approach, TMWE is 10 dB quieter than the baseline and 2 dB quieter than FMEQ. In all the analyzed flight regimes (takeoff, reduced thrust, acceleration, and supersonic cruise) the engine variants produced sufficiently high thrust levels while maintaining overall dimensions compatible with a supersonic airframe. The values of Specific Fuel Consumption at cruise and transonic acceleration are better than those of the Concorde engine. Of the two derivatives, TMWE has better overall noise performance and better fuel economy at cruise.

Refinements in nozzle shape are expected to enhance the benefit of TMWE. This is the subject of ongoing work in our laboratory.

Acknowledgments

The support by NASA Glenn Research Center is gratefully acknowledged (Grant NAG-3-2345 monitored by Dr. Khairul B. Zaman).

References

[1] Westley, R., and Lilley, G.M., "An Investigation of the Noise Field from a Small Jet and Methods for Its Reduction," College of Aeronautics, Rept. 53, Cranfield Univ., England, UK, Jan. 1952.

[2] Tam, C.K.W., and Chen, P., "Turbulent Mixing Noise from Supersonic Jets," *AIAA Journal*, Vol. 32, No. 9, 1994, pp. 1774-1780.

[3] Dahl, M.D. and Morris, P.J., "Noise from Supersonic Coaxial Jets, Part 2: Normal Velocity Profile," *Journal of Sound and Vibration*, Vol. 200, No. 5, 1997, pp. 665-699.

[4] Troutt, T.R., and McLaughlin, D.K., "Experiments on the Flow and Acoustic Properties of a Moderate Reynolds Number Supersonic Jet", *Journal of Fluid Mechanics*, Vol. 116, March 1982, pp. 123-156.

[5] Tam, C.K.W., Chen, P., and Seiner, J.M., "Relationship Between Instability Waves and Noise of High-Speed Jets", *AIAA Journal*, Vol. 30, No. 7, 1992, pp. 1747-1752.

[6] Seiner, J.M., Bhat, T.R.S, and Ponton, M.K., "Mach Wave Emission from a High-Temperature Supersonic Jet", *AIAA Journal*, Vol. 32, No. 12, 1994, pp. 2345-2350.

[7] Mitchell, B.E., Lele, S.K., and Moin, P., "Direct Computation of Mach Wave Radiation in an Axisymmetric Supersonic Jet," *AIAA Journal*, Vol. 35, No. 10, 1994, pp. 1574-1580.

[8] Powell, A., "On the Mechanism of Choked Jet Noise," *Proceedings of the Physical Society, London*, Vol. 66, 1953, pp. 1039-1056.

[9] Tam, C.K.W., "Supersonic Jet Noise,", *Annual Review of Fluid Mechanics,* Vol. 27, 1995, pp. 17-43.

[10] Raman, G., "Advances in Understanding Supersonic Jet Screech," AIAA Paper No. 98-0279, Jan. 1998.

[11] Harper-Bourne, M., and Fisher, M.J., "The Noise from Shock Waves in Supersonic Jets," *Proceedings of the AGARD Conference on Noise Mechanisms*, AGARD CP-131, 1973.

[12] Tam, C.K.W., "Stochastic Model Theory of Broadband Shock Associated Noise from Supersonic Jets," *Journal of Sound and Vibration*, Vol. 116, No. 2, 1987, pp. 265-302.

[13] Tillman, T.G., Paterson, R.W., and Presz, W.M., "Supersonic Nozzle Mixer Ejector", *AIAA Journal of Propulsion and Power*, Vol. 8, No. 2, 1992, pp. 513-519.

[14] Plencner, R.M., "Engine Technology Challenges for the High-Speed Civil Transport Plane", AIAA Paper No. 98-2505, 1998.

[15] Nagamatsu, H.T., Sheer, R.E., and Gill, M.S., "Characteristics of Multitude Multishroud Supersonic Jet Noise Suppressor", *AIAA Journal*, Vol. 10, No. 3, 1972, pp. 307-313.

[16] Papamoschou, D., "Analysis of Partially-Mixed Supersonic Ejector", *AIAA Journal of Propulsion and Power*, Vol. 12, No. 4, 1996, pp. 736-741.

[17] Knott, P.R., Stringas, E.J., Brausch, J.F., Staid, P.S., Heck, P.H., and Latham, D., "Acoustic Tests of Duct-Burning Turbofan Noise Simulation", NASA CR-2966, 1978.

[18] Tanna, H.K., Tester, B.J., and Lau, J.C., "The Noise and Flow Characteristics of Inverted-Profile Coannular Jets", NASA CR-158995, 1979.

[19] Olsen, W.A., and Friedman, R., "Jet Noise from Coaxial Nozzles over a Wide Range of Geometries and Flow Parameters", NASA TMX-71503, 1974.

[20] Majjigi, R.K., Brausch, J.F.D., Janardan, B.A., Balsa, T.F., Knott, P.R., and Pickup, N., "Free Jet Feasibility Study of a Thermal Acoustic Shield Concept for AST/VCE Application", NASA CR-3758, 1984.

[21] Papamoschou. D., "Mach Wave Elimination from Supersonic Jets", *AIAA Journal*, Vol. 35, No. 10, 1997, pp. 1604-1611.

[22] Papamoschou, D., "Method of Eliminating Mach Waves from Supersonic Jets," U.S. Patent No. 5590520, issued Jan. 7, 1997.

[23] Papamoschou, D., and Debiasi, M., "Noise Measurements in Supersonic Jets Treated with the Mach Wave Elimination Method," *AIAA Journal*, Vol. 37, No. 2, 1999, pp. 154-160.

[24] Debiasi, M., and Papamoschou, D., "Noise from Imperfectly Expanded Supersonic Coaxial Jets," *AIAA Journal*, Vol. 39, No. 3, 2001, pp. 388-395.

[25] Papamoschou, D., and Debiasi, M., "Directional Suppression of Noise from a High-Speed Jet," *AIAA Journal*, Vol. 39, No. 3, 2001, pp. 380-387.

[26] Debiasi, M., and Papamoschou, D., "Application of the Mach Wave Elimination Method to Supersonic Jet Engines," *Proceedings of the XIV International Symposium on Air Breathing Engines*, ISABE paper 99-7253, 1999.

[27] Murakami, E., and Papamoschou, D., "Eddy Convection in Coaxial Supersonic Jets", *AIAA Journal*, Vol. 38, No. 4, 2000, pp. 628-635.

[28] Murakami, E., and Papamoschou, D. "Mixing Layer Characteristics of Coaxial Supersonic Jets," AIAA-2000-2060.

[29] Sweetman, B., "YF-22 and YF-23 Advanced Tactical Fighters", Motorbooks International, 1991, Osceola, WI, pp. 61-64.

[30] Tanna, H.K., "Coannular Jets - Are They Really Quiet and Why?" *Journal of Sound and Vibration*, Vol. 72, No. 1, 1980, pp. 97-118.

[31] Hill, P., and Peterson, C., "Mechanics and Thermodynamics of Propulsion", 2nd Ed., Addison Wesley, 1992, New York.

[32] Kinzie, K.W., and McLaughlin, D.K., "Measurements of Supersonic Helium/Air Mixture Jets," *AIAA Journal,* Vol. 37, No. 11, 1999, pp. 1363-1369.

[33] "Jane's all the World Aircraft, 1998-1999", Sentinel House, 1998, Couldson UK.

[34] Hermann, P., "The EJ200 - Engine Development and Full Certification for Production Release with Eurofighter 2000", AIAA Paper No. 99-2661, 1999.

[35] Roth, B., and Mavris, D., "Analysis of Advanced Technology Impact on HSCT Engine Cycle", AIAA Paper No. 99-2379, 1999.

[36] Sanghi, V., and Lakshmanan, B.K., "Some Trends in Engine Cycle Selection and Overall Aircraft Sizing", *Proceedings of the XIV International Symposium on Air Breathing Engines*, ISABE paper 99-7112, 1999.

[37] Smith, M.J.T., "Aircraft Noise", 1st Ed., Cambridge University Press, 1989, Cambridge.

[38] Calder, P.H., and Gupta, P.C., "Future SST Engines with particular reference to Olympus 593 Evolution and Concorde Experience", SAE Paper No. 751056, 1975.

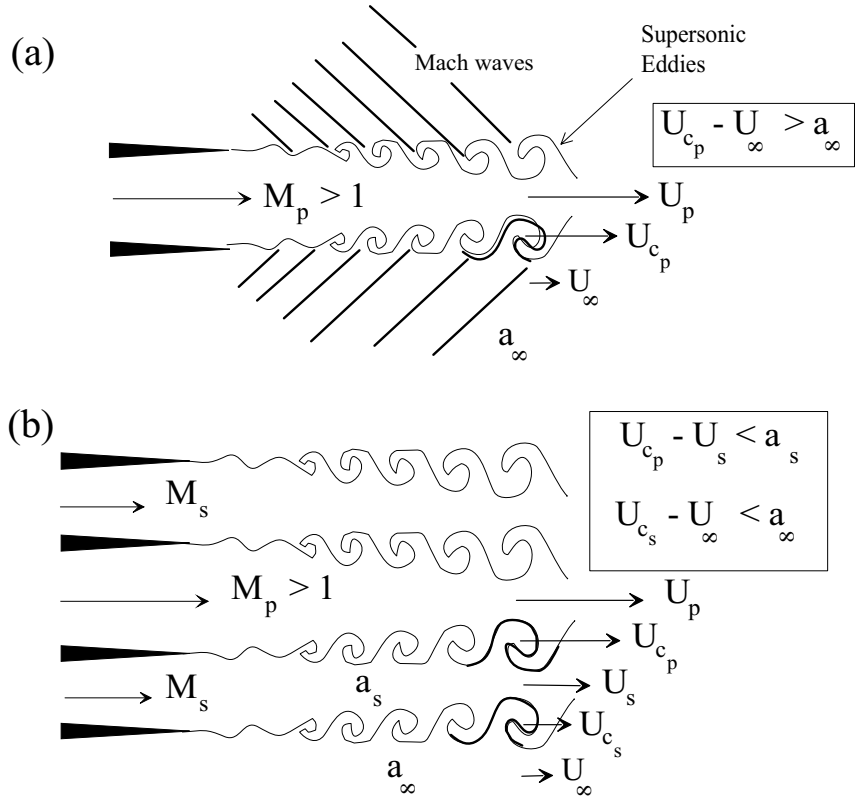

Figure 1: (a) Mach wave radiation in supersonic jets; (b) Principle of Mach Wave Elimination: creation of secondary flow adjacent to main jet so that all eddy motions become intrinsically subsonic.

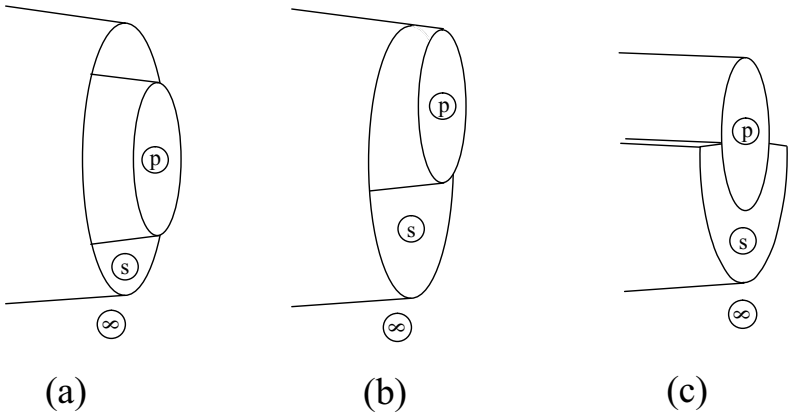

Figure 2: Nozzle configurations: (a) concentric; (b) eccentric; (c) arcuate.

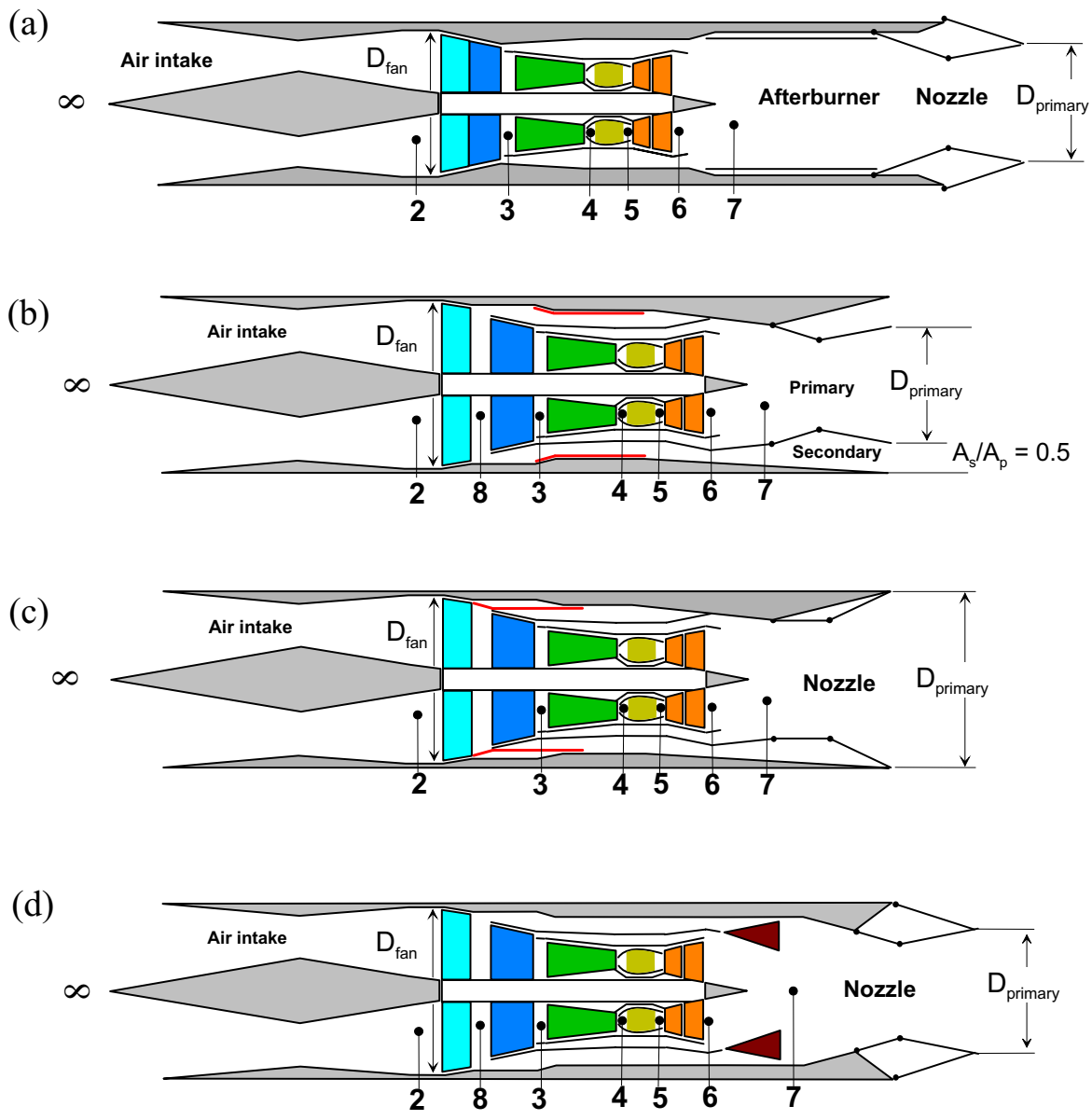

Figure 3: Turbofan engine configurations: (a) baseline engine; (b) two-stream TMWE at take-off thrust and reduced thrust; (c) single stream TMWE at high altitude flight; (d) FMEQ. The numbers correspond to different flow conditions in the engine cycle.

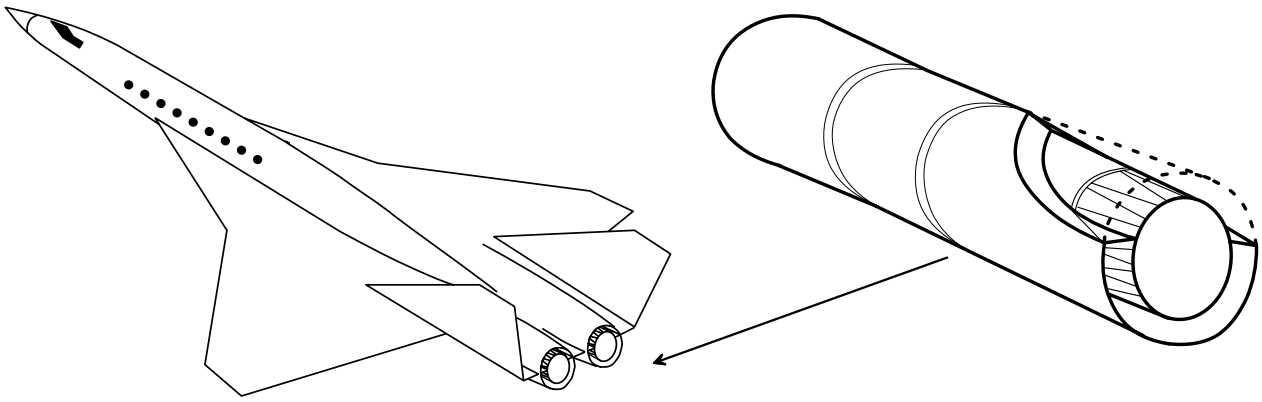

Figure 4: SSBJ concept incorporating TMWE turbofan engines.

Table 1: Parameters for turbofan engine cycle components (from Ref. [31]).

Component	Efficiency	Average specific heat ratio γ
air intake	$\eta = 0.97$	1.40
fan	$\eta = 0.85$	1.40
compressor	$\eta = 0.85$	1.37
combustor	$\eta = 1.00$	1.35
turbine	$\eta = 0.90$	1.33
jet nozzle	$\eta = 0.98$	1.36
fan nozzle	$\eta = 0.97$	1.4

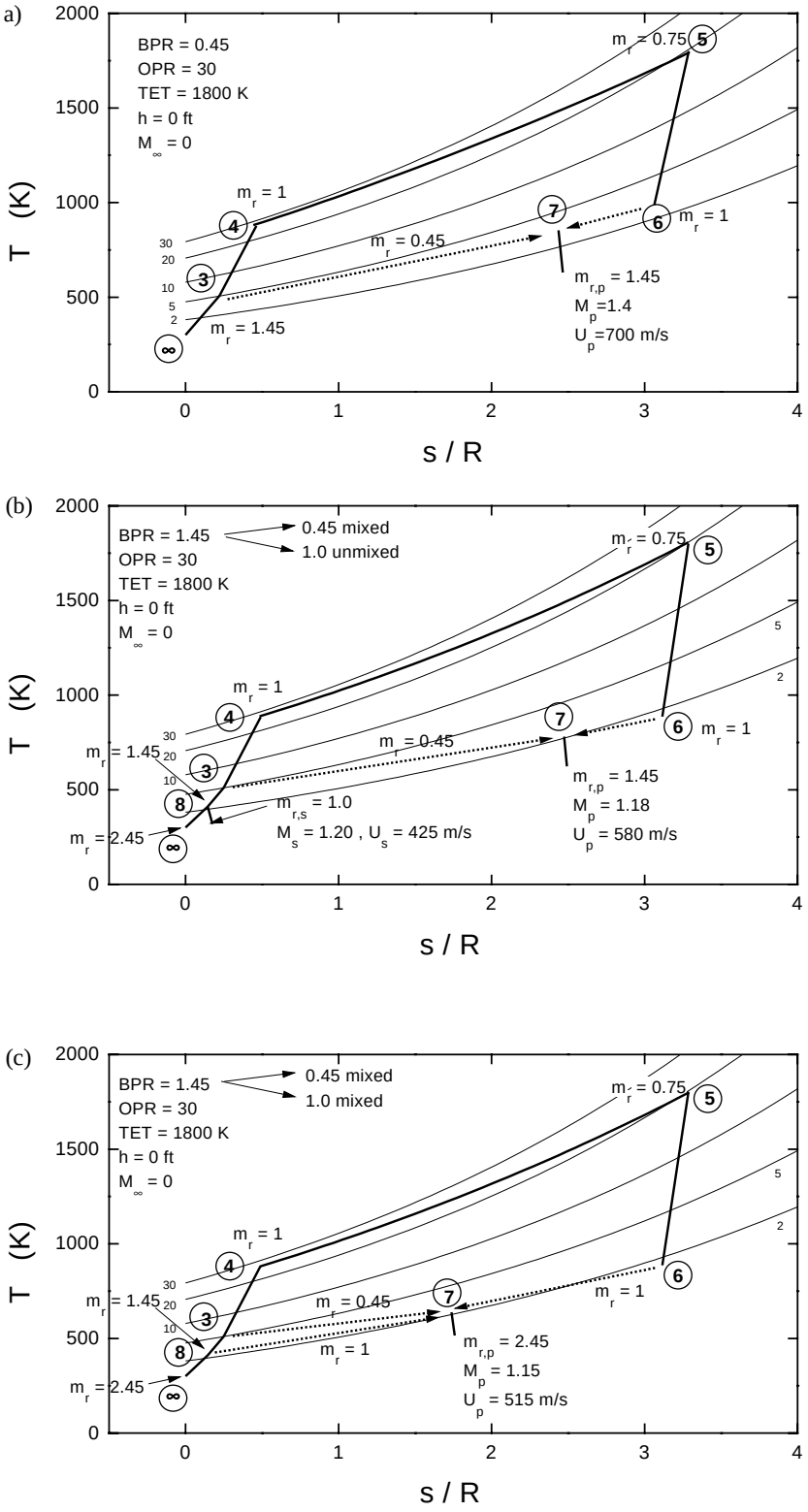

Figure 5: Take-off cycles for different engine configurations: (a) baseline; (b) TMWE; (c) FMEQ.

Table 2. Engine characteristics at full take-off thrust ($h = 0$ ft , $M_\infty = 0$).

	Baseline	TMWE	FMEQ
OPR [1]	30	30	30
TET [1][4] K (R)	1,800 (3,240)	1,800 (3,240)	1,800 (3,240)
$\dot{m}_{\rm com}$ [3] kg/s (lb/s)	96 (212)	94 (207)	94 (207)
$\dot{m}_{\rm tot}$ [3] kg/s (lb/s)	139 (307)	230 (507)	230 (507)
F [2] N (lbf)	100,000 (22,500)	120,000 (27,000)	120,000 (27,000)
BPR [2]	0.45 mixed	1.00 unmixed, 0.45 mixed	0.45 mixed + 1.00 mixed
FPR [1]	5.0	2.6 unmixed, 5.0 mixed	5.0 mixed + 2.6 mixed
$D_{\rm fan}$ [3][5] m	1.00	1.30	1.30
SFC [3] mg/N s (lb/lfb h)	17.8 (0.63)	14.4 (0.51)	14.4 (0.51)
M_p [2]	1.40	1.18	1.15
$U_{\rm p}$ [3] m/s (ft/s)	700 (2,300)	580 (1,900)	515 (1,700)
$D_{\rm p}$ [3] m	0.65	0.75	0.90
M_s [2]	-	1.20	-
$U_{\rm s}$ [3] m/s (ft/s)	-	425 (1,380)	-
$D_{\rm s}$ [3] m	-	0.89	-

(1) assumed; (2) datum; (3) computed; (4) with 25% compressor flow for blade cooling; (5) for $M_2 = 0.5$.

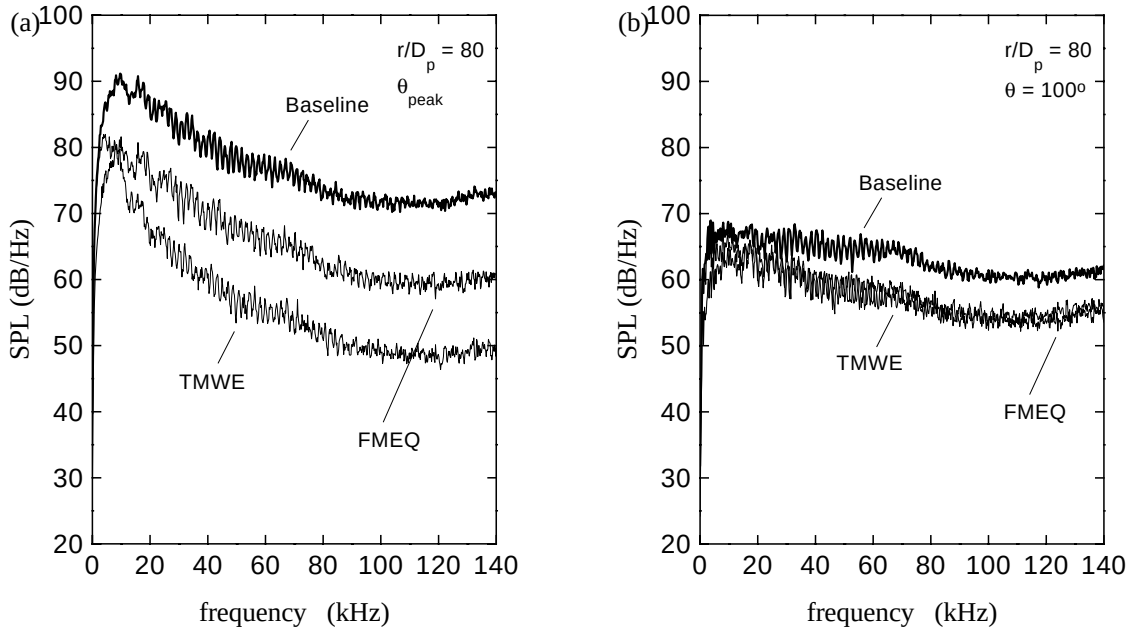

Figure 6: Narrowband, far-field spectra at full take-off thrust: (a) direction of peak emission: baseline ($\theta = 45^o$), TMWE ($\theta = 40^o$), and FMEQ ($\theta = 50^o$); (b) lateral direction ($\theta = 100^o$).

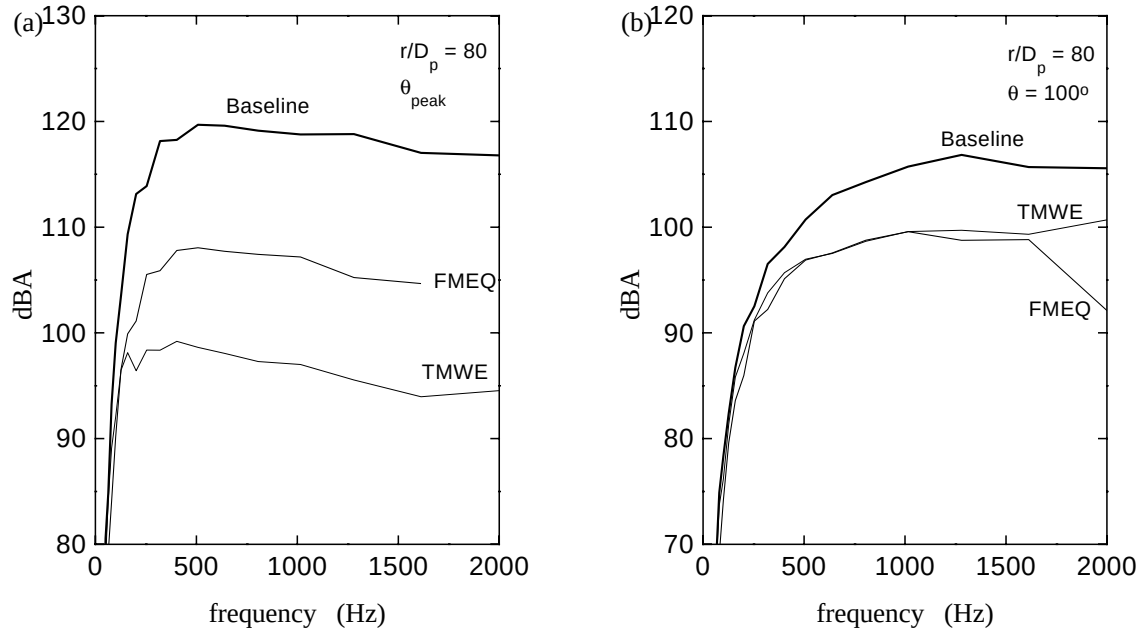

Figure 7: A-weighted, far-field spectra at full take-off thrust: (a) direction of peak emission: baseline ($\theta = 45^o$), TMWE ($\theta = 40^o$), and FMEQ ($\theta = 50^o$); (b) lateral direction ($\theta = 100^o$).

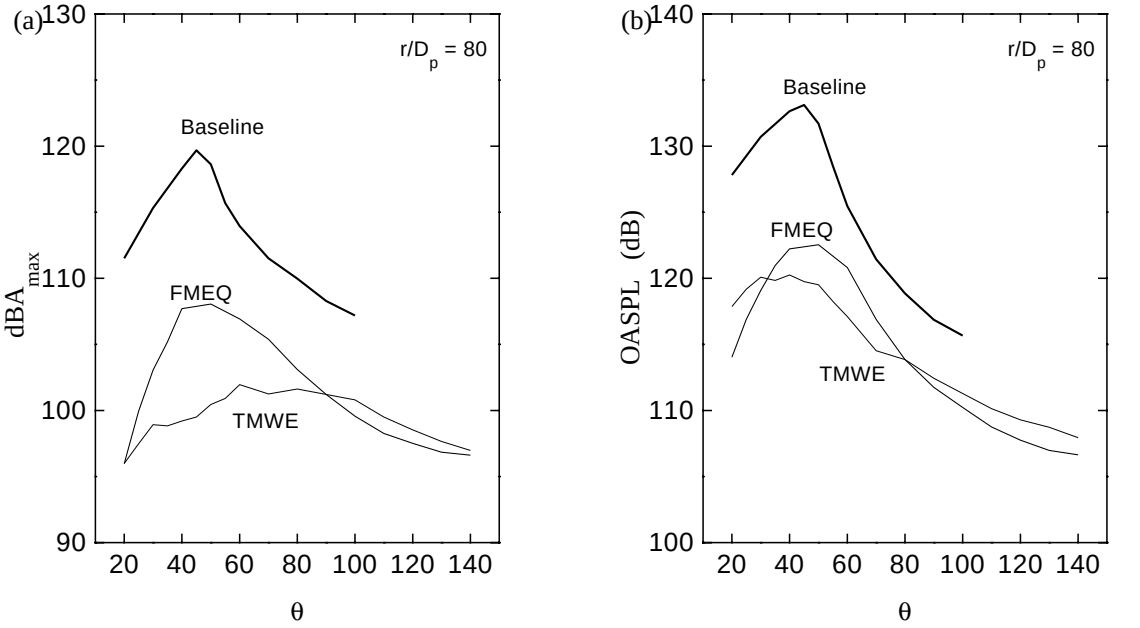

Figure 8: Directivities at full take-off thrust: (a) peak of dBA spectrum; (b) OASPL.

Table 3. Engine characteristics at reduced thrust ($h = 1{,}000$ ft , $M_\infty = 0.32$).

	Baseline	TMWE	FMEQ
OPR [1]	25	25	25
TET [1][4] K (R)	1,450 (2,610)	1,450 (2,610)	1,450 (2,610)
$\dot{m}_{\rm com}$ [3] kg/s (lb/s)	79 (174)	77 (169)	77 (169)
$\dot{m}_{\rm tot}$ [3] kg/s (lb/s)	115 (252)	189 (414)	189 (414)
F [2] N (lbf)	50,000 (11,250)	65,000 (14,500)	65,000 (14,500)
BPR [2]	0.45 mixed	1.00 unmixed, 0.45 mixed	0.45 mixed + 1.00 mixed
FPR [1]	4.3	1.8 unmixed, 4.3 mixed	4.3 mixed + 1.8 mixed
$D_{\rm fan}$ [3][5] m	1.00	1.30	1.30
SFC [3] mg/N s (lb/lfb h)	19.0 (0.67)	17.0 (0.60)	17.0 (0.60)
M_p [2]	1.20	1.12	1.05
$U_{\rm p}$ [3] m/s (ft/s)	550 (1,800)	530 (1,740)	450 (1,480)
$D_{\rm p}$ [3] m	0.65	0.70	0.90
M_s [2]	-	1.00	-
$U_{\rm s}$ [3] m/s (ft/s)	-	347 (1,140)	-
$D_{\rm s}$ [3] m	-	0.89	-

(1) assumed; (2) datum; (3) computed; (4) with 10% compressor flow for blade cooling; (5) for $M_2 = 0.4$.

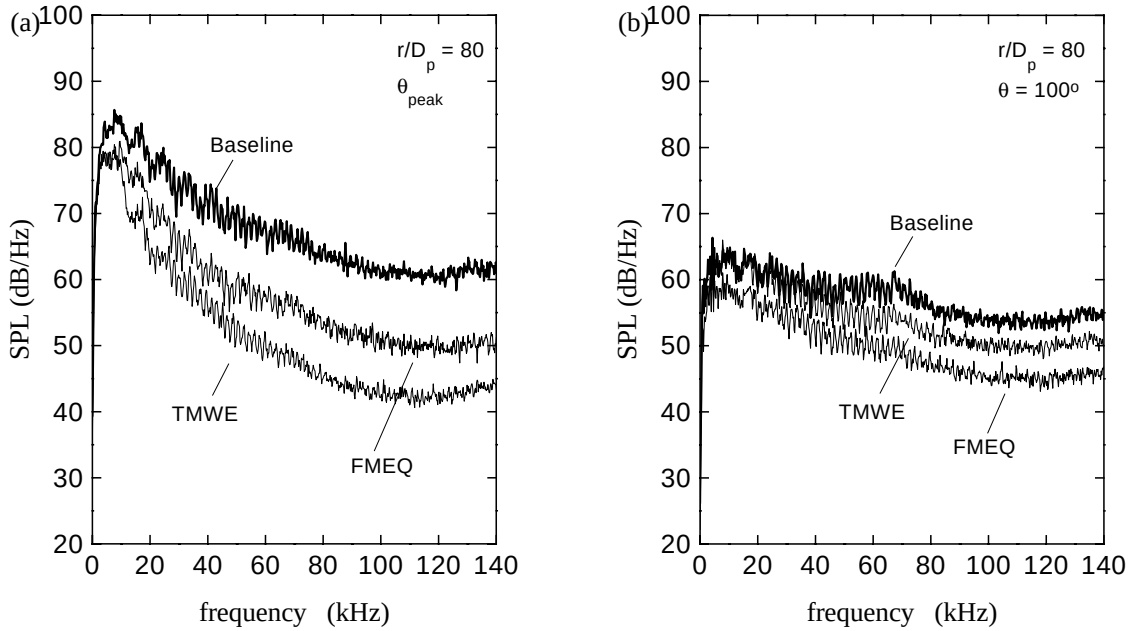

Figure 9: Narrowband, far-field spectra at reduced thrust: (a) direction of peak emission: baseline ($\theta = 35^o$), TMWE ($\theta = 40^o$), and FMEQ ($\theta = 25^o$); (b) lateral direction ($\theta = 100^o$).

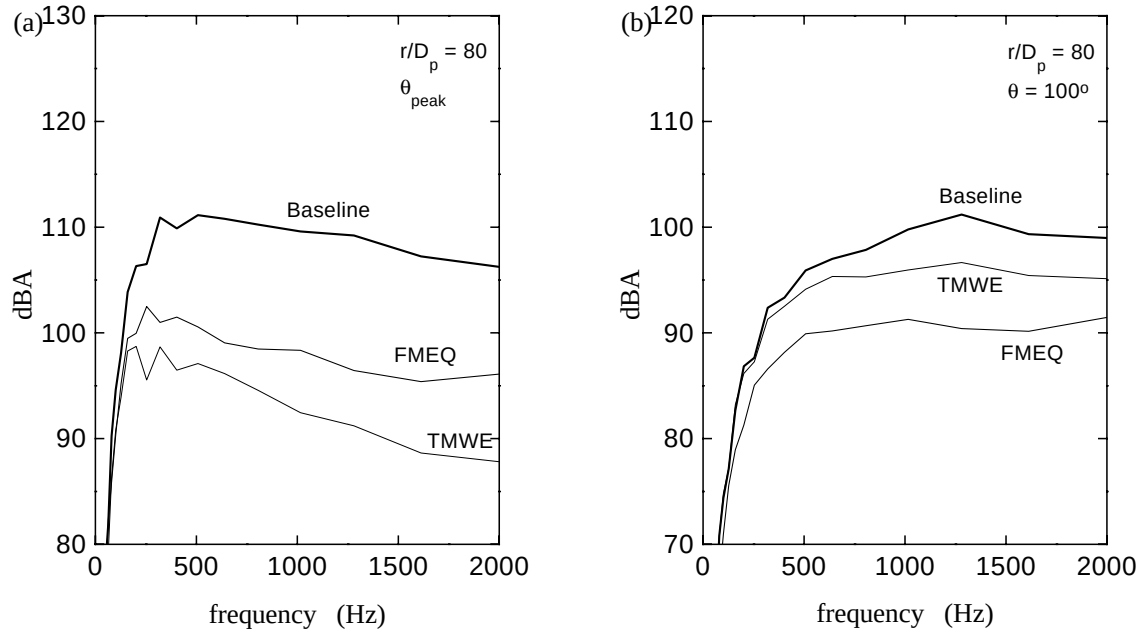

Figure 10: A-weighted, far-field spectra at reduced thrust: (a) direction of peak emission: baseline ($\theta = 35^o$), TMWE ($\theta = 40^o$), and FMEQ ($\theta = 25^o$); (b) lateral direction ($\theta = 100^o$).

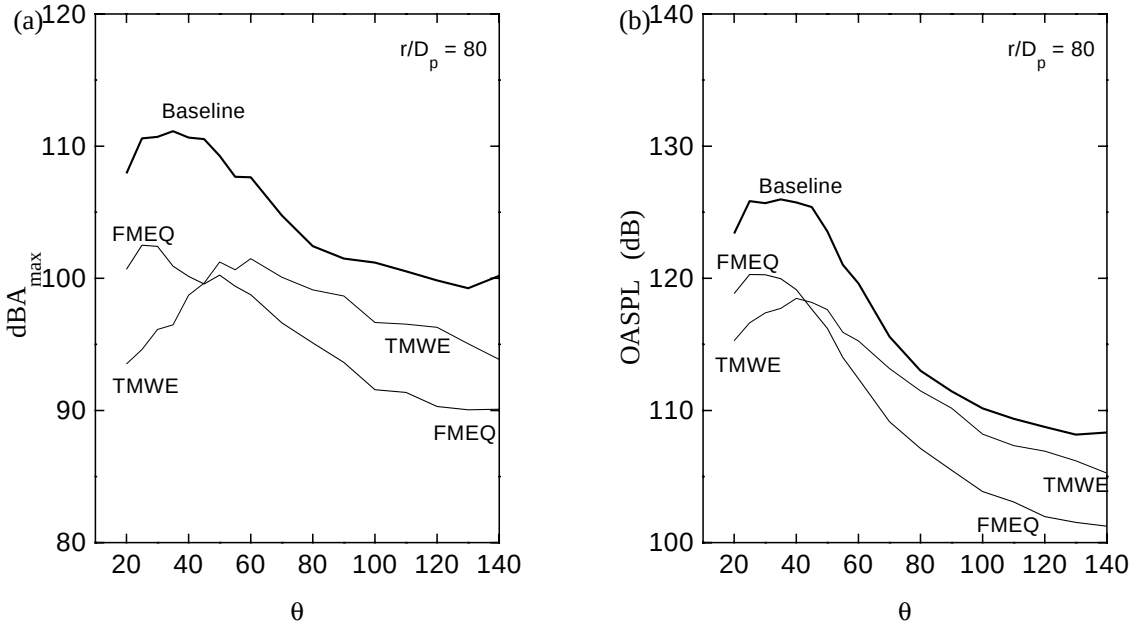

Figure 11: Directivities at reduced thrust: (a) peak of dBA spectrum; (b) OASPL.

Table 4. Engine characteristics at transonic acceleration ($h = 40,000$ ft , $M_\infty = 1.2$).

	Baseline	TMWE	FMEQ
OPR (1)	30	30	30
TET (1)(4) K (R)	1,800 (3,240)	1,800 (3,240)	1,800 (3,240)
$\dot{m}_{\rm com}$ (3) kg/s (lb/s)	66 (146)	92 (202)	54 (119)
$\dot{m}_{\rm tot}$ (3) kg/s (lb/s)	96 (218)	132 (292)	132 (292)
F (2) N (lbf)	50,000 (11,250)	70,000 (15,700)	45,000 (10,000)
BPR (2)	0.45 mixed	0.45 mixed	0.45 mixed + 1.00 mixed
FPR (1)	5.0	5.0 mixed	5.0 mixed + 2.6 mixed
$D_{\rm fan}$ (3)(5) m	1.00	1.30	1.30
SFC (3) mg/N s (lb/lfb h)	25.8 (0.91)	25.8 (0.91)	23.6 (0.84)
M_p (2)	1.90	1.90	1.70
$U_{\rm p}$ (3) m/s (ft/s)	860 (2,820)	860 (2,820)	688 (2,255)
$D_{\rm p}$ (3) m	1.00	1.20	1.25

(1) assumed; (2) datum; (3) computed; (4) with 25% compressor flow for blade cooling; (5) for $M_2 = 0.8$.

Table 5. Engine characteristics at cruise ($h = 50,000$ ft , $M_\infty = 2.0$).

	Baseline	TMWE	FMEQ
OPR (1)	25	25	25
TET (1)(4) K (R)	1,700 (3,060)	1,700 (3,060)	1,700 (3,060)
$\dot{m}_{\rm com}$ (3) kg/s (lb/s)	71 (157)	94 (207)	61 (134)
$\dot{m}_{\rm tot}$ (3) kg/s (lb/s)	103 (228)	136 (300)	149 (328)
F (2) N (lbf)	30,000 (6,750)	40,000 (9,000)	25,000 (5,600)
BPR (2)	0.45 mixed	0.45 mixed	0.45 mixed + 1.00 mixed
FPR (1)	4.5	4.5 mixed	4.5 mixed + 2.2 mixed
$D_{\rm fan}$ (3)(5) m	1.00	1.30	1.30
SFC (3) mg/N s (lb/lfb h)	28.9 (1.02)	28.9 (1.02)	29.9 (1.06)
M_p (2)	2.15	2.15	2.0
$U_{\rm p}$ (3) m/s (ft/s)	875 (2,870)	875 (2,870)	755 (2,475)
$D_{\rm p}$ (3) m	1.30	1.50	1.60

(1) assumed; (2) datum; (3) computed; (4) with 25% compressor flow for blade cooling; (5) for $M_2 = 0.6$.

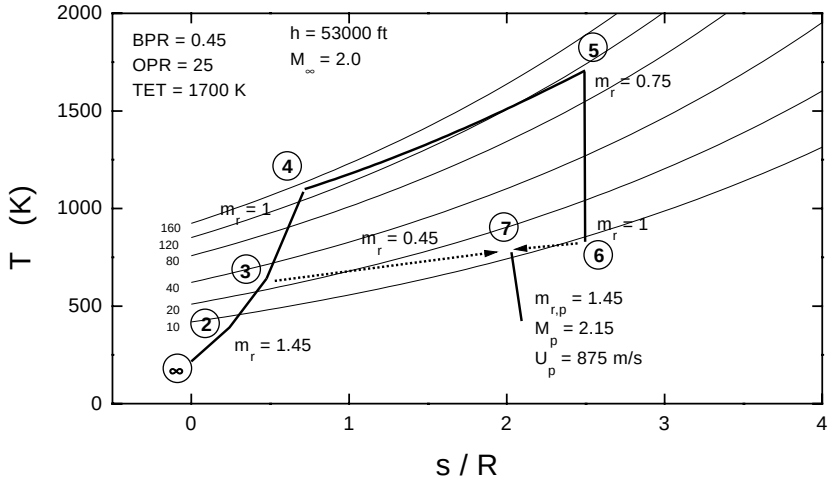

Figure 12: Cruise cycle for baseline and TMWE.